Chinese Chemical Letters 34 (2023) 107296

Contents lists available at ScienceDirect

Chinese Chemical Letters

journal homepage: www.elsevier.com/locate/cclet

Fine-tuning of pore-space-partitioned metal-organic frameworks for efficient C_2H_2/C_2H_4 and C_2H_2/CO_2 separation

Xiaobing Mu, Yingying Xue, Mancheng Hu*, Peng Zhang, Ying Wang, Haipeng Li, Shuni Li, Quanguo Zhai*

Key Laboratory of Macromolecular Science of Shaanxi Province, Key Laboratory of Applied Surface and Colloid Chemistry, Ministry of Education, School of Chemistry & Chemical Engineering, Shaanxi Normal University, Xi'an 710062, China

ARTICLE INFO

Article history:
Received 9 November 2021
Revised 12 February 2022
Accepted 3 March 2022
Available online 7 March 2022

Keywords:
Metal-organic framework
Pore space partition
C_2H_2 adsorption
C_2H_2/C_2H_4 separation
C_2H_2/CO_2 separation

ABSTRACT

Acetylene (C_2H_2) and ethylene (C_2H_4) both are important chemical raw materials and energy fuel gasses. But the effective removement of trace C_2H_2 from C_2H_4 and the purification of C_2H_2 from carbon dioxide (CO_2) are particularly challenging in the petrochemical industry. As a class of porous physical adsorbent, metal-organic frameworks (MOFs) have exhibited great success in separation and purification of light hydrocarbon gas. Herein, we rationally designed four novel MOFs by the strategy of pore space partition (PSP) *via* introducing triangular tri(pyridin-4-yl)-amine (TPA) into the 1D hexagonal channels of acs-type parent skeleton. By modulating the functional groups of linear dicarboxylate linkers for the parent skeleton, a series of isoreticular PSP-MOFs (SNNU-278–281) were successfully obtained. The synergistic effects of suitable pore size and Lewis basic functional groups make these MOFs ideal C_2H_2 adsorbents. The gas adsorption experimental results show that all MOFs have excellent C_2H_2 uptakes. Specially, SNNU-278 demonstrates a high C_2H_2 uptake of 149.7 cm^3/g at 273 K and 1 atm. Meanwhile, SNNU-278–281 MOFs also show extremely great C_2H_2 separation from CO_2 and C_2H_4. The optimized SNNU-281 with high-density hydroxy groups exhibits extraordinary C_2H_2/CO_2 and C_2H_2/C_2H_4 dynamic breakthrough interval times up to 31 min/g and 17 min/g under 298 K and 1 bar.

As the basic raw materials of petrochemical industry, acetylene (C_2H_2) and ethylene (C_2H_4) are usually produced by thermal cracking of hydrocarbons or combustion of natural gas [1]. In the process of producing C_2H_2, carbon dioxide (CO_2) is often contained as an impure substance, and traces of acetylene are often contained in the process of C_2H_4 production [2–4]. Therefore, it is very important to separate C_2H_2/CO_2 and C_2H_2/C_2H_4 binary gas mixtures. At present, distillation technology is used to separate mixed gases in industrial gas purification, but this technology has high energy consumption and high cost, which is not conducive to large-scale use [5]. Physical adsorption and separation based on porous adsorbents is supposed to greatly cut down energy consumption while achieving environmental protection.

Metal-organic frameworks (MOFs), also denoted as porous coordination polymers (PCPs), have emerged as a class of novel porous material self-assembled with metal ions/clusters and organic ligands [6,7]. In recent years, due to the distinctive characteristics of compositional diversity, large surface area, adjustable pore structure, and functional pore surface [8–12], MOFs have appeared as a promising class of porous materials in many fields, especially for the storage, separation and purification of small molecular gas [13–18]. According to the difference in gas mixtures (including size, shape and polarity of gas molecules) to design and synthesize MOF adsorbents is the key to achieve efficient gas separation performance [19,20]. For example, for C_2H_2 and C_2H_4 with different kinetic diameters (C_2H_2: 3.3 Å and C_2H_4: 4.2 Å), the size-based sieving strategy is effective for C_2H_2/C_2H_4 separation [21–24]. However, for CO_2 and C_2H_2 with similar kinetic diameters, it is necessary to introduce other functional sites such as functional ligands, open metal sites (OMS) and Lewis N sites to enhance the interaction between the C_2H_2 and skeleton [25–30]. Therefore, suitable pore size combine with the special binding sites in the frameworks of MOFs are considered to be more useful to enhance the adsorption discrimination for C_2H_2 over other gas.

Pore space partition (PSP) strategy is an effective method to control the pore size of MOFs. Herein, based on PSP strategy, a series of novel pacs (partition acs) MOFs were successfully synthesized by inserting symmetrical matching ligand into the hexago-

* Corresponding authors.
E-mail addresses: hmch@snnu.edu.cn (M. Hu), zhaiqg@snnu.edu.cn (Q. Zhai).

https://doi.org/10.1016/j.cclet.2022.03.019
1001-8417/

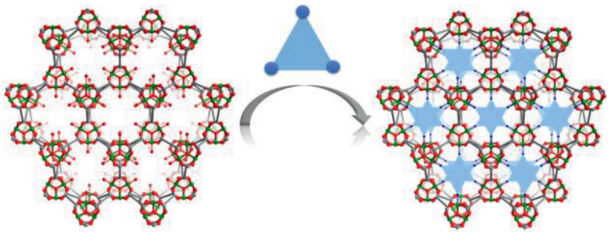

Scheme 1. Schematic representation of the PSP strategy.

nal channel of MIL-88-type (acs topology) framework (Scheme 1). By modulating the functional groups of dicarboxylic acid ligands of prototype framework, four isoreticular MOFs namely, $[Co_3(OH)L_3(TPA)]$ (SNNU-278: L = BDC; SNNU-279: L = NH_2BDC; SNNU-280: L = OHBDC; SNNU-281: L = DHBDC) were obtained. The combination of these structural features make these MOF materials not only show the excellent gas uptakes for C_2H_2, but also exhibit remarkable separation performance for C_2H_2/CO_2 and C_2H_2/C_2H_4 binary gas mixtures. The proper pore size coupled with high-density –OH groups make SNNU-281 demonstrates best dynamic breakthrough results for C_2H_2/CO_2 and C_2H_2/C_2H_4 separation.

All target MOF adsorbents were synthesized by solvothermal reactions with the mixtures of linear dicarboxylate ligands (BDC, NH_2BDC, OHBDC or DHBDC), tripyridine partitioner (TPA) and $Co(NO_3)_2{\cdot}6H_2O$ ultrasonically dissolved in mixed solvents of DMF, methanol and HBF_4 in a 20 mL glass vial. The mixtures were sealed and heated at 100 °C for 48 h. SNNU-278–281 were thus obtained as pink shuttle-shaped, red octahedral, light pink rod-shaped, and brown long shuttle-shaped crystals, respectively.

The single-crystal structure analysis uncovers that SNNU-278−281 are isostructural frameworks and crystallizes in the hexagonal $P6_3/mmc$ space group. Each Co center is six-coordinated in a octahedral geometry formed by four O atoms from four dicarboxylic acid ligands, one N atom from TPA, and one central μ_3–OH. Three Co atoms form the well-known trigonal prismatic $[Co_3(OH)]$ trimer, which is 9-connected with six dicarboxylic acid ligands and three TPA ligands. The $[Co_3(OH)]$ trimer units are extended to form MIL-88 type structures by six dicarboxylic acid ligands. When the three axial positions occupied by N atoms from TPA ligands, the 1D hexagonal channels along c-axis of MIL-88 were partitioned into numerous cylindrical segments of about 5.8 Å in length (Scheme 1). As shown in Fig. 1, the cylindrical cage (cage A) consist of six $[Co_3(OH)]$ trimer units, six dicarboxylic acid ligands and two TPA ligands. In addition, another kind of trigonal bipyramid-type cage (cage B) consist of five $[Co_3(OH)]$ trimer units, six dicarboxylic acid

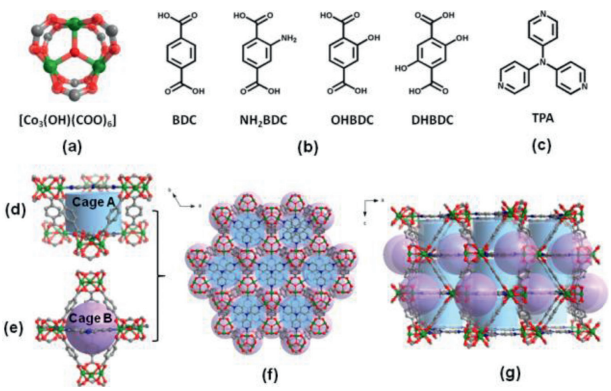

Fig. 1. The crystal structures for SNNU-278−281: (a) $[Co_3(OH)(COO)_6]$ cluster; (b) four linear dicarboxylate ligands; (c) triangular tri(pyridin-4-yl)-amine; (d, e) two types of cages; (f, g) 3D porous architecture viewed along the *c*-axis and *b*-axis directions.

ligands, and three TPA ligands (Figs. 1d and e). Each cage is adjacent to six another cages by sharing the vertexes and edges. The interlacing of two kinds of cages generate 3D porous framework of SNNU-278−281 (Figs. 1f and g).

The phase purity of all samples was determined by the powder X-ray diffraction (PXRD). As shown in Fig. S2 (Supporting information), the PXRD patterns of synthesized SNNU-278−281 MOFs match well with the simulated patterns from single-crystal data, which indicates the high crystallinity and good phase purities of all samples. Moreover, the isostructural architectures of SNNU-278−281 also verified by the PXRD. After soaking in different organic solvents for three days, the PXRD results of SNNU-278−281 compounds still are in good agreement with the as-prepared samples, which demonstrate their good chemical stability (Fig. S3 in Supporting information) Meanwhile, the thermal stability of SNNU-278−281 were measured by thermogravimetric analysis (TGA). As shown in Fig. S4 (Supporting information), the as-prepared and CH_3CN-exchanged samples all can be stable up to at least 300 °C under N_2 atmosphere. Compared with the as-prepared samples, the TGA curves of the activated samples have more obvious platform. A continuous weight loss of ~20% from 25 °C to ~100 °C are observed for activated samples of SNNU-278−281, corresponding to the loss of trapped solvent molecules. Then the MOF skeletons can keep stable until 380, 340, 350 and 300 °C for SNNU-278−281, respectively. With the rising of temperature, two continuous weight losses are observed, corresponding to the escape of organic ligands.

To evaluate the permanent porosities of SNNU-278−281, N_2 adsorption isotherms were measured on their activated samples at 77 K. These as-synthesized materials were activated by immersion in CH_3CN for 4 days and then were heated at 80 °C for 10 h under a dynamic vacuum. The PXRD patterns of samples after gas sorption measurements matches well with that of the as-synthesized samples, indicating that the activated samples retained structures stability (Fig. S2). As shown in Fig. 2a, SNNU-278−281 show reversible type-I isotherms of the microporous materials. The maximum N_2 adsorptions for SNNU-278−281 at 77 K are 304, 293, 277 and 254 cm^3/g and their pore volumes are 0.46, 0.40, 0.39 and 0.38 cm^3/g, respectively. The corresponding Brunauer−Emmett−Teller (BET) surface areas of SNNU-278−281 are estimated to be 830, 750, 730 and 710 m^2/g and Langmuir surface areas are estimated to be 1340, 1180, 1150 and 1110 m^2/g, respectively. The pore size distributions reveal that sharp peaks centered at 4.25 Å by the Horvath−Kawazoe method.

The porous properties and regulated functional sites prompted us to further investigate the gas adsorption and separation of SNNU-278−281 for small gas molecules. As shown in Fig. 2b, the C_2H_2 uptakes for SNNU-278−281 under 1 atm are 149.7/109.9, 139.5/106.5, 133.4/102.9, and 123.7/92.7 cm^3/g at 273/298 K, respectively. Even if the C_2H_2 uptakes for SNNU-278−281 are not the best, these values are much higher than many famous MOF adsorbents, such as UPC-110 (131.7 cm^3/g) [31], JU-26 (127 cm^3/g) [32], UTSA-222a (103.4 cm^3/g) [33], JXNU-5 (70.3 cm^3/g) [34]. The C_2H_2 uptake capacities at 1 bar follow the order of SNNU-278 > SNNU-279 > SNNU-280 > SNNU-281, which are consistent with the order of pore volumes. However, the C_2H_2 uptakes of SNNU-279−281 are higher than SNNU-278 at lower pressure (<0.1 bar), which attributed to the strong force between functional groups (–NH_2 and –OH) and C_2H_2 molecules.

Furthermore, at 273/298 K and 1 atm, the C_2H_4 uptakes for SNNU-278−281 also show the same tendency. As shown in Fig. 2c, the corresponding values are 119.9/90.0 cm^3/g, 110.3/86.4 cm^3/g, 103.1/79.4 cm^3/g and 93.0/73.4 cm^3/g, respectively. Notably, the CO_2 uptake capacity of these four MOFs show very slight difference at 273/298 K and 1 atm (Fig. 2d). They can adsorb 125.8/74.1, 128.1/80.2, 126.5/76.2 and 125.0/78.0 cm^3/g, respectively. In detail,

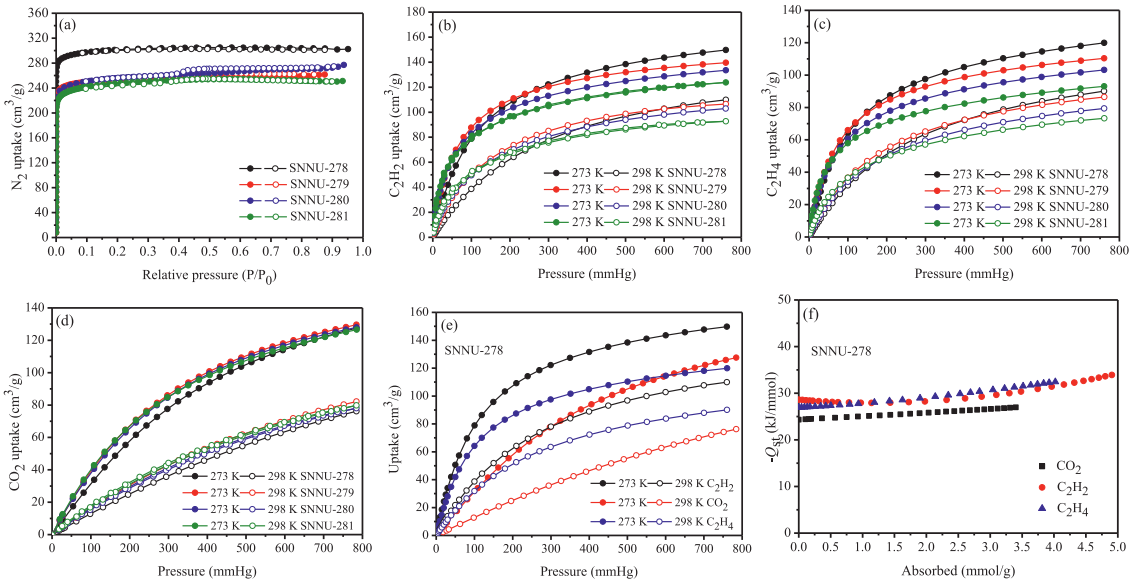

Fig. 2. Gas adsorption performance for SNNU-278–281: (a) N_2 sorption isotherms at 77 K; (b) C_2H_2 uptake isotherms at 273 K and 298 K; (c) C_2H_4 uptake isotherms at 273 K and 298 K; (d) CO_2 uptake isotherms at 273 K and 298 K; (e) CO_2, C_2H_2 and C_2H_4 uptake isotherms at 273 K and 298 K for SNNU-278; (f) isosteric heats of gas adsorption (Q_{st}) for SNNU-278.

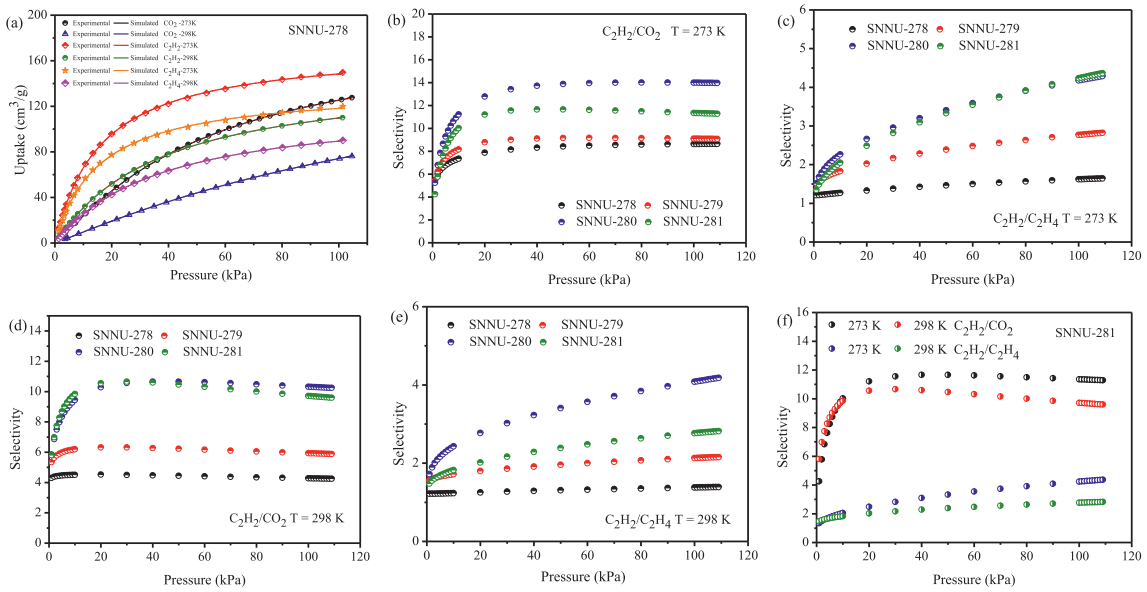

Fig. 3. The selectivities predicted for equimolar binary mixtures by IAST of SNNU-278–281: (a) adsorption isotherms of simulated by IAST and experimental for SNNU-278; the comparison of selectivities of all MOFs for (b) C_2H_2/CO_2 at 273 K, (c) C_2H_2/C_2H_4 at 273 K, (d) C_2H_2/CO_2 at 298 K, and (e) C_2H_2/C_2H_4 at 298 K; (f) C_2H_2/CO_2 and C_2H_2/C_2H_4 at 273 K and 298 K for SNNU-281.

the uptake capacity of SNNU-278–281 for C_2H_2 are higher than those for C_2H_4 and CO_2 (Fig. 2e and Fig. S5 in Supporting information). Meanwhile, under low pressure (<0.2 bar), the gas uptakes for these MOFs follow the order of C_2H_2 > C_2H_4 > CO_2, indicating the immense potential of C_2H_2/C_2H_4 and C_2H_2/CO_2.

The isosteric heat (Q_{st}) was further calculated to assess the interaction between SNNU-278–281 materials and small gas molecules. As depicted in Fig. 2f, the $-Q_{st}^0$ values of C_2H_2, C_2H_4 and CO_2 at zero-coverage on SNNU-278 are 28.6, 26.9 and 24.3 kJ/mol. The corresponding values are 33.4/35.5/33.1, 27.6/28.8/26.9 and 25.8/33.7/25.7 kJ/mol for SNNU-279–281 (Fig. S6 in Supporting information). Obviously, the $-Q_{st}^0$ values of these MOFs for C_2H_2 are higher than C_2H_4 and CO_2, which further suggest the frameworks have stronger interaction with C_2H_2 molecules. Moreover, it is noted that SNNU-279–281 show higher $-Q_{st}^0$ values over SNNU-278, proving again the function of –NH_2 and –OH groups on small gas molecules.

To evaluate the separation performance for SNNU-278–281, the ideal adsorbed solution theory (IAST) method was used to predict the adsorption selectivity. According to Langmuir–Freundlich (LF) approach, the experimental gas isotherms are well fitted with the simulation results at 273 K and 298 K (Fig. 3a). As shown in Figs. 3b and d, under 1 atm, the IAST selectivities of SNNU-278–281 for the equimolar C_2H_2/CO_2 are 8.6, 9.1, 14.0, and 11.3 at 273 K and 4.3, 5.9, 10.2 and 9.6 at 298 K, respectively. The corresponding values are 1.6, 2.8, 4.3 and 4.4 at 273 K and 1.4, 2.2, 4.2 and 2.8 at 298 K for the equimolar C_2H_2/C_2H_4 (Figs. 3c and e). In comparison, the functional groups of –NH_2 and –OH make the selectivities

Table 1
CO_2, C_2H_2 and C_2H_4 uptake amounts (cm^3/g) and IAST selectivity values of equimolar binary C_2H_2/CO_2 and C_2H_2/C_2H_4 mixtures for SNNU-278–281.

MOFs	Uptake (cm^3/g)						IAST selectivity			
	273 K			298 K			273 K		298 K	
	CO_2	C_2H_2	C_2H_4	CO_2	C_2H_2	C_2H_4	C_2H_2/CO_2	C_2H_2/C_2H_4	C_2H_2/CO_2	C_2H_2/C_2H_4
SNNU-278	125.8	149.7	119.9	74.1	109.9	90.0	8.6	1.6	4.3	1.4
SNNU-279	128.1	139.5	110.3	80.2	106.5	86.4	9.1	2.8	5.9	2.2
SNNU-280	126.5	133.4	103.1	76.2	102.9	79.4	14.0	4.3	10.2	4.2
SNNU-281	125.0	123.7	93.0	78.0	92.7	73.4	11.3	4.4	9.6	2.8

of SNNU-279–281 superior to SNNU-278. And the values of SNNU-280 and SNNU-281 are clearly higher than SNNU-279, which is due to the stronger force of –OH for C_2H_2 over $-NH_2$ (Table 1).

In addition, all MOFs show better separation performance for C_2H_2/CO_2 than C_2H_2/C_2H_4, demonstrating that the frameworks interact with gas molecules in the order of C_2H_2 > C_2H_4 > CO_2, which is consistent with the gas adsorption C_2H_2 results (Fig. 3f and Table 1). Remarkably, at 298 K and 1 atm, the C_2H_2/CO_2 selectivity values for SNNU-280 and SNNU-281 are much higher than some promising MOF adsorbents under the same conditions, such as $Cu(BDC\text{-}Br)(H_2O)_{0.5}(DMF)_{2.0}$ (3.9) [35], $Cu_2(ade)_2(PA)_2$ (4.2) [36], FJU-90a (4.3) [37], ZJNU-93a (4.5) [38], ZJNU-76a (4.7) [39], MUF-17 (6.0) [2].

In order to further verify the practical separation performance of C_2H_2/CO_2 and C_2H_2/C_2H_4 for these MOFs, the breakthrough curves were tested. For equimolar binary gas mixtures C_2H_2/CO_2 and C_2H_2/C_2H_4, the experimental results show that CO_2 and C_2H_4 first eluted and then C_2H_2 was retained until its saturated uptake (Figs. S7 and S8 in Supporting information). As shown in Fig. 4a, at 298 K and 1 atm, the breakthrough time toward C_2H_2/CO_2 mixtures are 17, 22, 29 and 31 min/g for SNNU-278–281 with a flow rate of 2.0 mL/min, respectively. The corresponding values are 10, 12, 14 and 17 min/g toward C_2H_2/C_2H_4 mixtures under the same conditions (Fig. 4b). By comparison, the breakthrough time for SNNU-280 and SNNU-281 is longer than that of SNNU-278 and SNNU-279, which indicates the introduction of –OH groups is beneficial to separate C_2H_2/CO_2 and C_2H_2/C_2H_4. The breakthrough residue times of SNNU-281 clearly surpass many other MOFs such as ZJU-196a (6.3 min/g) [40], UTSA-300a (12.8 min/g) [41], FJU-90a (22 min/g) [37] and UTSA-74a (27 min/g) (Fig. 4d) [42].

The reproducibility and recyclability of the adsorbent is another important parameter to evaluate its practical adsorption and separation performance. Therefore, the recycle breakthrough experiments of SNNU-281 for C_2H_2/CO_2 were also tested under a flow rate of 4.0 mL/min. As shown in Fig. 4c, SNNU-281 shows good recyclability after three dynamic breakthrough experiments, indicating the structural stability of the adsorbent. These breakthrough results further demonstrate that these PSP-MOFs are promising porous materials for C_2H_2/CO_2 and C_2H_2/C_2H_4 separation.

To clearly know the interaction between gas molecules and MOFs, Grand Canonical Monte Carlo (GCMC) was used to simulate gas molecules distribution and favorable sorption site within the MOF skeleton at 298 K. As depicted in Figs. S9a-f (Supporting information), these results show that the distribution density of C_2H_2 is much higher than that of CO_2 for different frameworks, which is consistent with result of adsorption capacity. For C_2H_2 adsorption of the SNNU-281, main adsorption sites are located at the pore space, indicating that TPA ligand provide affinity site to C_2H_2. In addition, -OH group also provide stronger interactions of OH···CH≡CH (Fig. S9g in Supporting information). It is noted that several kinds of hydrogen bonds between C_2H_2 and the MOF skeleton in SNNU-281 are observed. The bond lengths are about 3.99 Å, 3.29 Å, 3.26 Å and 2.57 Å, and bond angles range from 110° to 136°, respectively. But the CO_2 adsorption sites for SNNU-281 are less in the pore compared to C_2H_2 (Fig. S9h in Supporting information). Therefore, it can be concluded that suitable pore space and func-

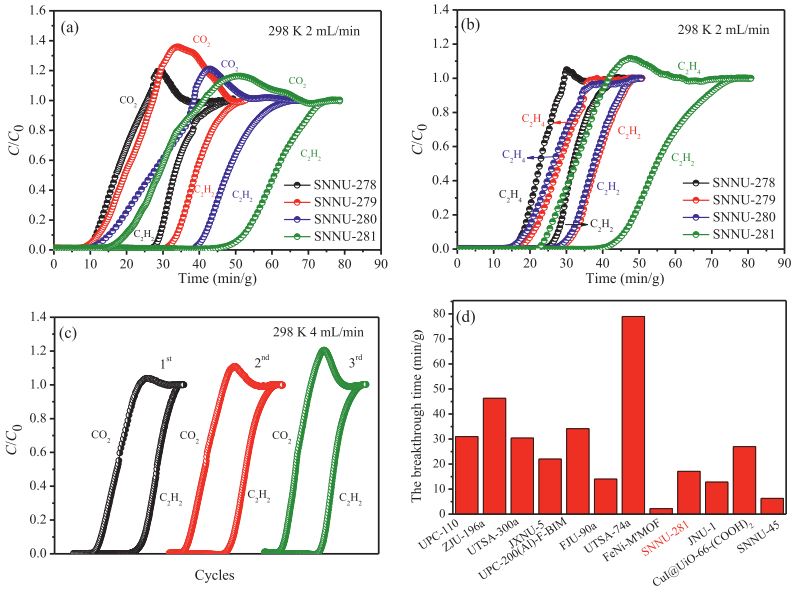

Fig. 4. (a) The experimental breakthrough curves of SNNU-278–281 for the C_2H_2/CO_2 (50:50) at 298 K and 1 atm. (b) The experimental breakthrough curves of SNNU-278–281 for the C_2H_2/C_2H_4 (50:50) at 298 K and 1 atm. (c) The cycling test of SNNU-281 at 298 K for the equimolar C_2H_2/CO_2. (d) Comparison of the breakthrough residue times for equimolar C_2H_2/CO_2 at 298 K and 1 atm of some best MOF adsorbents.

tional groups play important role to improve separation property of C_2H_2/CO_2.

In summary, we successfully designed four novel isoreticular MOFs with targeted topological nets by utilizing the pore space partition (PSP) strategy. All MOFs show excellent gas adsorption and separation performance, and the C_2H_2 uptake amount of SNNU-278 is superior to most famous MOFs. The gas adsorption and GCMC simulations all indicate that introduction of Lewis basic groups are clearly beneficial for the C_2H_2/CO_2 and C_2H_2/C_2H_4 separation performance. Specially, the optimized SNNU-281 with high-density –OH groups demonstrates the longest dynamic breakthrough residue time among four pore-space-partitioned metal-organic framework adsorbents.

Declaration of competing interest

We declared that we have no conflicts of interest to this work.

Acknowledgments

This work is financially supported by the National Natural Science Foundation of China (No. 22071140), the Natural Science Foundation of Shaanxi Province (No. 2021JLM-20), the Fundamental Research Funds for the Central Universities (No. GK202101002).

Supplementary materials

Supplementary material associated with this article can be found, in the online version, at doi:10.1016/j.cclet.2022.03.019.

References

[1] G.F. Hua, X.J. Xie, W. Lu, D. Li, Dalton Trans. 49 (2020) 15548–15559.
[2] O.T. Qazvini, R. Babarao, S.G. Telfer, Chem. Mater. 31 (2019) 4919–4926.
[3] X.P. Fu, Y.L. Wang, Q.Y. Liu, Dalton Trans. 49 (2020) 16598–16607.
[4] R.B. Lin, S. Xiang, W. Zhou, B. Chen, Chem 6 (2020) 337–363.
[5] Y. Du, Y. Chen, Y. Wang, et al., Sep. Purif. Technol. 256 (2021) 117749–117755.
[6] B. Li, H.M. Wen, Y. Cui, et al., Adv. Mater. 28 (2016) 8819–8860.
[7] W. Lu, Z. Wei, Z.Y. Gu, et al., Chem. Soc. Rev. 43 (2014) 5561–5593.
[8] C. Li, L. Zhang, J. Chen, et al., Nanoscale 13 (2021) 485–509.
[9] J. Wang, Q. Zhu, Z. Zhang, et al., Angew. Chem. 133 (2021) 2–9.
[10] M.Y. Masoomi, A. Morsali, A. Dhakshinamoorthy, H. Garcia, Angew. Chem. Int. Ed. 58 (2019) 15188–15205.
[11] M. Ding, X. Cai, H.L. Jiang, Chem. Sci. 10 (2019) 10209–10230.
[12] N. Stock, S. Biswas, Chem. Rev. 112 (2012) 933–969.
[13] H. Daglar, H.C. Gulbalkan, G. Avci, et al., Angew. Chem. Int. Ed. 60 (2021) 7828–7837.
[14] W. Fan, X. Wang, B. Xu, et al., J. Mater. Chem. A 6 (2018) 24486–24495.
[15] D. Alezi, Y. Belmabkhout, M. Suyetin, et al., J. Am. Chem. Soc. 137 (2015) 13308–13318.
[16] T. Grancha, M. Mon, J. Ferrando-Soria, et al., J. Mater. Chem. A 5 (2017) 11032–11039.
[17] Y. Wang, W. Fan, X. Wang, et al., Inorg. Chem. Front. 5 (2018) 2408–2412.
[18] Y. Wang, X. Wang, X. Wang, et al., Cryst. Growth Des. 19 (2018) 832–838.
[19] F. Zheng, L. Guo, B. Gao, et al., ACS Appl. Mater. Inter. 11 (2019) 28197–28204.
[20] R.B. Lin, H. Wu, L. Li, et al., J. Am. Chem. Soc. 140 (2018) 12940–12946.
[21] Y. Huang, Y. Xu, B. Zheng, et al., Energy Fuels 34 (2020) 11315–11321.
[22] B. Li, X. Cui, D. O'Nolan, et al., Acta Mater. 29 (2017) 1704210–1704216.
[23] X. Jiang, T. Pham, J.W. Cao, et al., Chem. Eur. J. 27 (2021) 9446–9453.
[24] J. Wang, Y. Zhang, P. Zhang, et al., J. Am. Chem. Soc. 142 (2020) 9744–9751.
[25] W. Gong, H. Cui, Y. Xie, et al., J. Am. Chem. Soc. 143 (2021) 14869–14876.
[26] W. Fan, S.B. Peh, Z. Zhang, et al., Angew. Chem. Int. Ed. 60 (2021) 17338–17343.
[27] H.M. Wen, H. Wang, B. Li, et al., Inorg. Chem. 55 (2016) 7214–7218.
[28] W. Fan, S. Yuan, W. Wang, et al., J. Am. Chem. Soc. 142 (2020) 8728–8737.
[29] W. Fan, X. Zhang, Z. Kang, X. Liu, D. Sun, Coord. Chem. Rev. 443 (2021) 213968–214024.
[30] W. Fan, X. Wang, X. Zhang, et al., ACS Cent. Sci. 5 (2019) 1261–1268.
[31] W. Fan, X. Wang, X. Liu, et al., ACS Sustainable Chem. Eng. 7 (2018) 2134–2140.
[32] X. Duan, J. Cai, J. Yu, et al., Micropor. Mesopor. Mater. 181 (2013) 99–104.
[33] J.X. Ma, J. Guo, H. Wang, et al., Inorg. Chem. 56 (2017) 7145–7150.
[34] R. Liu, Q.Y. Liu, R. Krishna, et al., Inorg. Chem. 58 (2019) 5089–5095.
[35] H. Cui, Y. Ye, H. Arman, et al., Cryst. Growth Des. 19 (2019) 5829–5835.
[36] H. Li, H. Bonduris, X. Zhang, et al., J. Solid State Chem. 284 (2020) 121209–121212.
[37] Y. Ye, Z. Ma, R.B. Lin, et al., J. Am. Chem. Soc. 141 (2019) 4130–4136.
[38] S. Li, J. Wu, X. Gao, et al., CrystEngComm 20 (2018) 7178–7183.
[39] F. Chen, D. Bai, Y. Wang, et al., Mater. Chem. Front. 1 (2017) 2283–2291.
[40] L. Zhang, K. Jiang, L. Li, et al., Chem. Commun. 54 (2018) 4846–4849.
[41] R.B. Lin, L. Li, H. Wu, et al., J. Am. Chem. Soc. 139 (2017) 8022–8028.
[42] F. Luo, C. Yan, L. Dang, et al., J. Am. Chem. Soc. 138 (2016) 5678–5684.